Algorithmic Design of Low-Power Variable-Stiffness Mechanisms

Vincent Chalvet and David J. Braun

***Abstract*—Compliant actuators enabling low-power stiffness adaptation are missing ingredients and key enablers of next generation robotic systems. One of the key components of these actuators is the mechanism implementing stiffness adaptation that requires sophisticated control and nontrivial mechanical design. However, despite recent advances in controlling these systems, their design remains experience based and not well understood. In this paper, we present an optimization-based computational framework for the design of intrinsically low-power compliant variable stiffness mechanisms. The core ingredient of this framework is the mathematical formulation of the design problem—provided by a constrained nonlinear parameter optimization—which is computationally solved here to identify optimal variable stiffness designs. We show the basic capability of this formulation in finding parameters for variable stiffness mechanisms that require the least power by design. Further, we demonstrate the generality of this method in cross-comparing mechanisms with different kinematic topology to identify the one that requires the least power by design.**

***Index Terms*—Computational design, optimization-based design, variable stiffness.**

I. Introduction

Compliant actuators used to implement stiffness modulation are actuators characterized by passive and tunable force-deflection relation. This is achieved by a dedicated variable stiffness mechanism that introduces compliance, physical and geometric nonlinearity as well as control redundancy by design [1]. Depending on the task considered, these actuators may be designed for large-enough modulation range and high-enough bandwidth; both required in practical applications [2]–[7]. However, despite a number of successful implementations of this concept, the task relevant advantage these actuators can deliver is often hindered by the energy cost they require. There have been numerous attempts to address this issue by developing mathematical frameworks [8]–[10], and novel compliant actuators [11]–[13] capable of low-power stiffness modulation. Nevertheless, the principles underlying the design of these systems are not well understood. As a result, there is currently no systematic framework for energetically efficient compliant actuator design.

Mechanical design has been long perceived principally rooted in *experience-based* cognition, i.e., it is the experience that enables the engineer to convert the creative and innovative ideas to a practical design [14]. However, ever since the introduction of computational kinematics [15], first principles based automatic design has been recognized a future goal [16]. This has led to two important developments in the field of computer-aided design; one of these is provided by a systematic approach to motion syntheses of rigid kinematic mechanisms [17] while another is topological optimization that enables optimal computational design of static compliant mechanical structures [18]. Design of compliant mechanisms is typically focused on transformation from a given input motion to a desired output motion, either by using rigid body mechanisms endowed with concentrated compliance, or by considering continuum mechanisms for which structural optimization is performed [19]. Despite these investigations, the concept of inherently low-power mechanical design, its mathematical formulation, and computational treatment has yet to be demonstrated.

Here, we present an optimization-based computational approach for the design of intrinsically low-power compliantly actuated systems. To focus on the main challenge, we consider the design of variable stiffness mechanisms that have been long perceived energy hungry, limiting the utility of stiffness modulation as a means of actuation, and the autonomy of variable stiffness robots, for decades [8], [11], [20]. The core component of our design approach—and the main contribution of this paper—is the mathematical formulation and the computational treatment of intrinsically low-power variable stiffness design. The resulting constrained, nonlinear, possibly nonconvex and nonsmooth optimization problem can be computationally solved to define both the kinematic structure and the parameters of the optimal design. We show the basic capability of this formulation in finding parameters for variable stiffness mechanisms that require low power due to their design. Further, we demonstrate the generality of this method in cross-comparing mechanisms with different kinematic topology to identify the one that requires the least power by design.

The proposed approach differs from typical rigid kinematic and compliant static algorithmic design frameworks in two important ways. First, unlike input–output motion synthesis that leads to a mechanical design suitable for a particular use, our approach leads to a power minimal, i.e., energetically optimal design regardless of its particular use. Second, unlike a more conventional decoupled sequential dimensional and kinematic type synthesis, the two are inherently coupled and simultaneously treated in our computational design.

In Section II, we introduce the basic formulation of the optimization-based design problem using a minimalistic example. This is followed by the complete mathematical formulation in Section III. Application of this formulation is demonstrated in Section IV on three qualitatively different compliant mechanisms; all three optimized to be energetically efficient by design. In Section V, we exemplify a computational cross-comparison between two of these mechanisms to identify the one that requires less power by design. Finally, in Section VI, we use the proposed computational framework to optimize the design of an existing variable stiffness mechanism.

The proposed formulation is shown to enable a systematic treatment of a difficult global optimization problem underlying simultaneous topological and parametric synthesis of intrinsically low-power compliant mechanisms.

Manuscript received February 6, 2017; accepted May 27, 2017. Date of publication August 21, 2017; date of current version December 14, 2017. This paper was recommended for publication by Associate Editor S. Kim and Editor I.-M. Chen upon evaluation of the reviewers' comments. This work was funded by the SUTD-MIT International Design Center at the Singapore University of Technology and Design, as a part of the Energy-Efficient Compliant Actuator Designs Project under Grant IDG31400108. *(Corresponding author: David J. Braun.)*

The authors are with the Dynamics and Control Laboratory, Engineering Product Development Pillar at Singapore University of Technology and Design, Singapore 487372 (e-mail: david_braun@sutd.edu.sg; vincent_chalvet@sutd.edu.sg).

Color versions of one or more of the figures in this paper are available online at http://ieeexplore.ieee.org.

Digital Object Identifier 10.1109/TRO.2017.2719049

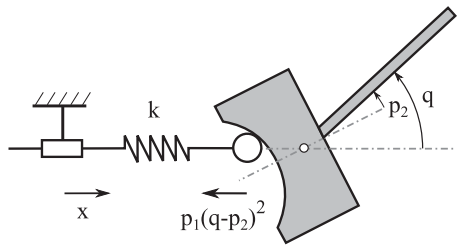

Fig. 1. Schematic representation of a variable stiffness cam mechanism. In this mechanism k denotes the stiffness of the linear spring, q is the output angle, x is the input position while (p_1, p_2) denote the transmission ratio of the cam and the offset of the output link.

II. Dimensional Synthesis: Minimalistic Example

Figure 1 shows a minimalistic variable stiffness mechanism, representative of pre-tension/compression-based mechanisms [5], [21]. The output position of this mechanism is denoted with q, whereas the input position is denoted with x. In this design, the roller moving in a nonlinear cam is connected to a spring that generates the apparent stiffness of the joint. The motor acts directly on the spring by compressing it, and as such, changing the stiffness of the joint. The mechanism is characterized by a simple mathematical model, parameterized by the cam transmission ratio p_1, and the offset of the output link p_2 (see Fig. 1). We use this simple example to introduce the mathematical formulation and to exemplify a closed form analytical design optimization.

The potential energy function of this mechanism is given by

$$V(x, q; \mathbf{p}) = \frac{1}{2} k \left(x + p_1 \left(q - p_2 \right)^2 \right)^2 \tag{1}$$

where k denotes the stiffness of the spring while $\mathbf{p} = (p_1, p_2)$ represents the design parameters (see Fig. 1).

There are two generic quantifiers of this and other variable stiffness mechanisms; one is the output stiffness, which is motor position dependent (i.e., changeable by changing x):

$$K_{\text{out}}(x, q; \mathbf{p}) = \frac{\partial^2 V}{\partial q^2} = 2 p_1 k \left(x + 3 p_1 (q - p_2)^2 \right) \tag{2}$$

while the other is the input force imposed by the stiffness modulating mechanism on the motor, given by

$$F_{\text{in}}(x, q; \mathbf{p}) = -\frac{\partial V}{\partial x} = -k \left(x + p_1 \left(q - p_2 \right)^2 \right). \tag{3}$$

The power required to change the output stiffness is given by [22]:

$$P_{\text{in}}(x, \dot{x}, \ddot{x}, q; \mathbf{p}) = P_0(x, \dot{x}, \ddot{x}) + (w_1 \ddot{x} + w_2 \dot{x}) F_{\text{in}} + w_3 F_{\text{in}}^2 \tag{4}$$

where P_0 is the power required by the stiffness modulating motor when it is not restrained by the mechanism ($F_{\text{in}} = 0$) while w_i, $i \in \{1, 2, 3\}$ are positive constants that depend on the physical parameters of the drive train connecting the motor and the stiffness modulating mechanism.

The first component on the right-hand side of (4) represents the power drained to change the stiffness independent of the load at the output, the second component represents the additional power due to the tuning mechanism, whereas the last component is the power required to hold a desired stiffness. One of the key observation here is that, regardless of the particular use of the mechanism (i.e., regardless of how the device is controlled), the power input can be effectively reduced by minimizing the magnitude of the input force [1] [22]. In particular, when $F_{\text{in}} = 0$, the power is reduced to the one required to drive the motor when it is not connected to the variable stiffness mechanism.

Following this observation, we propose to minimize the squared input force with respect to the design parameters

$$\mathbf{p}^* = \underset{\mathbf{p} \in \mathcal{P}_0}{\operatorname{argmin}} \overline{F_{\text{in}}^2}(\mathbf{p}) \tag{5}$$

where $\mathcal{P}_0$ is the user-defined admissible range of the design parameters while

$$\overline{F_{\text{in}}^2}(\mathbf{p}) = \frac{\iint_{\mathcal{S}(\mathbf{p})} F_{\text{in}}(x, q; \mathbf{p})^2 \left| \frac{\partial K_{\text{out}}}{\partial x} \right| dx dq}{\iint_{\mathcal{S}(\mathbf{p})} \left| \frac{\partial K_{\text{out}}}{\partial x} \right| dx dq} \tag{6}$$

is the input force averaged over the user defined workspace.[2] In the simplest form, this workspace is given by

$$\mathcal{S}(\mathbf{p}) = \{(x, q) \in \mathcal{X}_0 \times \mathcal{Q}_0 : K_{\text{out}}(x, q; \mathbf{p}) \in \mathcal{K}_0\} \tag{7}$$

where $\mathcal{X}_0$, $\mathcal{Q}_0$, and $\mathcal{K}_0$ are user-defined ranges of the input motion x, output motion q, and the output stiffness K_{out}. This nonlinear parameter optimization problem, i.e., (5)–(7), provides the mathematical representation of the optimization-based mechanical design.

Assuming that the set of admissible design parameters is not constrained $\mathcal{P}_0 = \mathbb{R}^2$ and that the workspace of the mechanism is $\mathcal{S}(\mathbf{p}) = \{(x, q) \in \mathbb{R} \times [q_m, q_M] : K_m \leqslant K_{\text{out}}(x, q; \mathbf{p}) \leqslant K_M\}$, the solution of the above optimization problem is given by

$$\mathbf{p}^* = \left[\left(\frac{5}{3} \frac{K_m^2 + K_m K_M + K_M^2}{k^2 (q_M - q_m)^4} \right)^{\frac{1}{4}}, \frac{q_M + q_m}{2} \right]. \tag{8}$$

The obtained solution is the global minimum of (5)–(7), which provides the parameters for the optimal design. The corresponding mechanism is indeed a variable stiffness mechanism, since irrespective of the parameter values (8), the output stiffness remains motor position dependent, see (2).

Typically, design optimization is considered to be a process where the design parameters are optimized for one particular task. In the present context, this could be done by optimizing the parameters along one specific path in the output motion-stiffness workspace. The present formulation extends this task specific optimization by considering a range of acceptable motions and a range of acceptable stiffness values. This kind of generalization is essential when it comes to variable stiffness designs. This is because, variable stiffness systems are not designed for one particular task but to realize variety of tasks where stiffness could be adapted under *a priori* unknown external conditions.

III. Dimensional Synthesis: Mathematical Formulation

Following the above consideration, the optimal design is the one that leads to minimal static power consumed by the driving motor over the entire workspace of the mechanism. We stress that, this is achieved by minimizing the magnitude of the input force which, in turn, reduces the total power required for stiffness modulation, see (4).

The optimal design process is broken down to two sequential optimization problems. The first of these problems (I) is used to find the

[1] The size of the electric motor, driving the variable stiffness mechanism, is determined by the motor torque and not the motor power. A mechanism for which the magnitude of F_{in} is minimized will lead to reduced motor torque in a similar way as it leads to reduced motor power. This is because when $F_{\text{in}} = 0$, the mechanism does not increase the motor torque.

[2] The averaging is defined over the output position and output stiffness space, i.e., $\iint F_{\text{in}}^2 dK dq / \iint dK dq$.

largest feasible workspace of the mechanism. Within this largest feasible workspace, the user selects a *desired workspace* of interest which is the input to the second optimization. The second optimization problem (II) minimizes the average squared input force imposed on the motor over the user-defined desired workspace. The final result provides the parameters that define the optimal mechanical design. The mathematical formulation of this two stage optimal dimensional synthesis is given in the following:

- Provide the parameterized model of the mechanism, i.e., specify the elastic potential energy function

$$V = V(x, q; \mathbf{p}).$$

- Provide the set of design parameters $\mathbf{p} \in \mathcal{P}_0 \subset \mathbb{R}^n$.
- Provide the input workspace $(x, q) \in \mathcal{X}_0 \times \mathcal{Q}_0 \subset \mathbb{R}^2$.
- Provide the region of interest for the output stiffness

$$K_{\text{out}}(x, q; \mathbf{p}) \in \mathcal{K}_0 \subset \mathbb{R}.$$

- Provide the design constraints (e.g., physical constraints due to deformation and stress limits of the elastic elements)[3]

$$\mathbf{c}(x, q; \mathbf{p}) \preceq \mathbf{0}.$$

- Define the feasible workspace of the mechanism

$$\mathcal{S}(\mathbf{p}) = \{(x, q) \in \mathcal{X}_0 \times \mathcal{Q}_0 : K_{\text{out}}(x, q; \mathbf{p}) \in \mathcal{K}_0, \mathbf{c}(x, q; \mathbf{p}) \preceq \mathbf{0}\}.$$

(I) *Largest feasible workspace:* Find the parameters $\mathbf{p}_{\max}$ that maximize the area of the feasible workspace

$$\mathbf{p}_{\max} = \underset{\mathbf{p} \in \mathcal{P}_0}{\operatorname{argmax}} \iint_{\mathcal{S}(\mathbf{p})} \left| \frac{\partial K_{\text{out}}}{\partial x}(x, q; \mathbf{p}) \right| dx dq. \tag{9}$$

- Provide the feasible desired workspace in the output stiffness output position space $\mathcal{S}_{\text{d,out}}$

$$\mathcal{S}_{\text{d, out}} \subseteq \mathcal{S}_{\text{out}}(\mathbf{p}_{\max}) \subset \mathcal{K}_0 \times \mathcal{Q}_0 \tag{10}$$

such that it is contained by the largest feasible workspace $\mathcal{S}_{\text{out}}(\mathbf{p}_{\max})$ defined in the output stiffness output position space[4]

$$\mathcal{S}_{\text{out}}(\mathbf{p}) = \{(K_{\text{out}}(x, q; \mathbf{p}), q) \in \mathcal{K}_0 \times \mathcal{Q}_0 : (x, q) \in \mathcal{S}(\mathbf{p})\}. \tag{11}$$

(II) *Optimal design parameters:* Find the design parameters that minimize the squared input force over the user selected desired workspace

$$\mathbf{p}^* = \underset{\mathbf{p} \in \mathcal{P}_0 : \mathcal{S}_{\text{d}}(\mathbf{p}) \subseteq \mathcal{S}(\mathbf{p})}{\operatorname{argmin}} \frac{\iint_{\mathcal{S}_{\text{d}}(\mathbf{p})} F_{\text{in}}(x, q; \mathbf{p})^2 \left| \frac{\partial K_{\text{out}}}{\partial x} \right| dx dq}{\iint_{\mathcal{S}_{\text{d}}(\mathbf{p})} \left| \frac{\partial K_{\text{out}}}{\partial x} \right| dx dq} \tag{12}$$

where[5] $\mathcal{S}_{\text{d}}(\mathbf{p}) = \{(x, q) \in \mathcal{X}_0 \times \mathcal{Q}_0 : (K_{\text{out}}(x, q; \mathbf{p}), q) \in \mathcal{S}_{\text{d, out}}\}$ is the user-defined desired workspace represented in the input position output position space $\mathcal{X}_0 \times \mathcal{Q}_0$.

The solution of this nonlinear constrained optimization problem provides the parameters $\mathbf{p}^*$ that define an intrinsically low-power mechanical design.[6]

[3] $\preceq$ denotes elementwise inequality relations.

[4] By knowing the feasible workspace which has the largest area $\mathcal{S}_{\text{out}}(\mathbf{p}_{\max})$, the user is able to choose variety a feasible desired workspaces $\mathcal{S}_{\text{d, out}} \subseteq \mathcal{S}_{\text{out}}(\mathbf{p}_{\max})$ for the considered mechanism.

[5] This optimization problem involves a *set inclusion constraint*. While this constraint is an atypical one, it can be implemented using inequality constrained algebraic relations.

[6] Any user selected feasible desired workspace $\mathcal{S}_{\text{d, out}} \subseteq \mathcal{S}_{\text{out}}(\mathbf{p}_{\max})$ ensures existence of at least one feasible solution (i.e., $\mathbf{p}^* = \mathbf{p}_{\max}$) of (12).

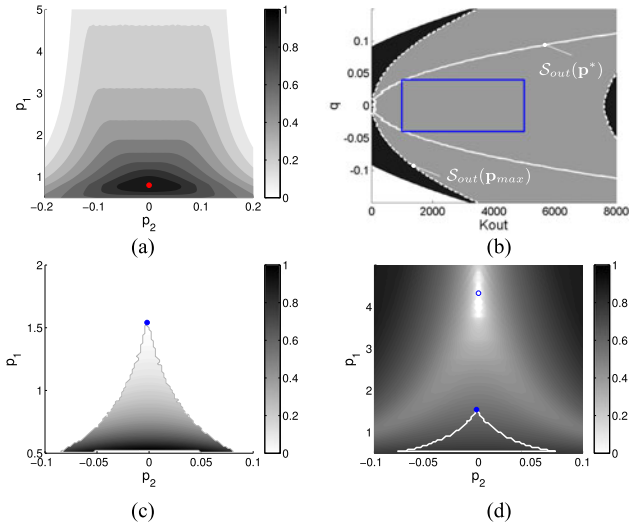

Fig. 2. (a) Area of the feasible workspace as a function of the design parameters. The parameters $\mathbf{p}_{\max}$ that correspond to the largest area are indicated by the red dot. (b) Largest feasible workspace (gray area) and desired workspace selected by the user (blue box). The optimal feasible workspace is represented with a white line. (c) Value of the cost function (squared input force averaged over the desired workspace) as a function of the design parameters. The optimal parameters found by the algorithm correspond to the blue dot. (d) Comparison of the constrained solution (blue dot) and the unconstrained solution (blue circle). The triangular shapes in the last two plots define the set of feasible design parameters.

IV. Computational Design Optimization

In this section, we demonstrate the use of the above mathematical formulation to find optimal design parameters for three qualitatively different variable stiffness mechanisms. In all three mechanisms, physical feasibility is assured by taking into account the deformation and stress limits during the optimization. In the first example, we revisit the mechanism presented in Section II to demonstrate the effect of physical constraints on the optimal design. This example will be followed by two other, more complex, mechanisms. The results reported here are obtained by solving the mathematical formulation outlined in Section III, using numerical optimization.

A. Variable Stiffness Cam Mechanism

As a first example, we revisit the design optimization presented in Section II, see Fig. 1. The parameterized model of the cam mechanism, considered in Section II, is provided by (1). However, unlike in Section II, here we take into account the physical limitations, according to which the design of the cam mechanism should be realized using a compression spring that has a finite deformation limit. This physical limitation is given by

$$\delta(x, q; \mathbf{p}) \in [0, 0.08] \tag{13}$$

where $\delta(x, q; \mathbf{p}) = x + p_1 (q - p_2)^2$ denotes the deformation of the spring. In order to complete this formulation, the range of design parameters and the workspace of the mechanism are defined by

$$\mathcal{P}_0 = [0.5, 5] \times [-0.2, 0.2] \text{ and}$$
$$\mathcal{X}_0 \times \mathcal{Q}_0 \times \mathcal{K}_0 = [-0.02, 0.1] \times [-0.15, 0.15] \times [0, 8000]. \tag{14}$$

Given these settings, the area of the feasible workspace is maximized. This is done by solving the first optimization problem (9). The result of this optimization is shown in Fig. 2(a). The figure rep-

resents the area of the feasible workspace as a function of the design parameters. The red dot corresponds to the largest area and defines the associated design parameters $\mathbf{p} = \mathbf{p}_{\max}$. The largest feasible workspace $\mathcal{S}_{\text{out}}(\mathbf{p}_{\max}) \subseteq \mathcal{K}_0 \times \mathcal{Q}_0$ is shown in Fig. 2(b)[7] (gray area). Once the largest feasible workspace is known, the user can select the desired workspace: $\mathcal{S}_{\text{d, out}} = [1000, 5000] \times [-0.04, 0.04]$, blue box in Fig. 2(b). This workspace should be entirely feasible, i.e., it should satisfy the following proposition: $\exists \mathbf{p} \in \mathcal{P}_0 : \mathcal{S}_{\text{d, out}} \subseteq \mathcal{S}_{\text{out}}(\mathbf{p})$. This condition is assured if the desired workspace (blue box) is contained by the largest feasible workspace (gray area), as shown in Fig. 2(b).

Using the user-defined desired workspace $\mathcal{S}_{\text{d, out}}$, we proceed to solve the second optimization problem (12). The result of this optimization is shown in Fig. 2(c). This figure represents the value of the average squared input force per workspace as a function of the feasible design parameters. The set of feasible design parameters has a triangular shape. The parameters that provide the optimal mechanical design, in presence of the deformation limits (13), correspond to the blue dot in Fig. 2(c). These parameters are on the boundary of the feasible set.

For comparison, Fig. 2(d) shows the cost $\overline{F_{\text{in}}^2}(\mathbf{p})$ as a function of the design parameters $\mathcal{P}_0$. This plot shows the set of feasible parameters (white triangular shape), the optimal design parameters (blue dot), and the optimal solution (8) (blue circle) obtained without taking into account the deformation limit of the spring (13). We can observe that when the deformation limits are considered, the algorithm finds a feasible solution (blue dot) that is the closest to the solution obtained without taking the deformation limits into account (blue circle).

According to this result, the optimal design for the chosen workspace requires positive transmission ratio $p_1^* > 0$, and no cam offset $p_2^* = 0$, see Fig. 2(d). Finding the value of the first parameter may not be trivial without optimization even in this simple example. On the other hand, the second parameter could have been intuitively found by an experienced designer even without optimization because the desired workspace is symmetric in this example. The algorithm verifies this intuition using numerical computation.

The total cost associated with the optimal mechanism ($\mathbf{p} = \mathbf{p}^*$) is the quarter of the cost associated with the nonoptimized mechanism (i.e., the one which has the largest feasible workspace $\mathbf{p} = \mathbf{p}_{\max}$)

$$\overline{F_{\text{in}}^2}(\mathbf{p}^*)/\overline{F_{\text{in}}^2}(\mathbf{p}_{\max}) \approx 0.25.$$

It is interesting to note that the considered design problem is not only nonlinear and constrained but can be nonconvex—see Fig. 2(c)—and possibly nonsmooth. In order to numerically solve such optimization problem, we use constraint consistent initialization and nongradient-based search optimization.

B. Variable Stiffness Slider Mechanism

As a next example, we consider a variable stiffness slider mechanism shown in Fig. 3(a). This mechanism is similar to number of practical designs [11], [23] that employ the adjustable moment arm principle. Compared to other practical designs, this mechanism possesses certain kinematic generalization introduced for design optimization. The mentioned kinematic generalization relates to the introduction of two design parameters. The first parameter p_1 is the pretension of the springs (same for both springs), whereas the second parameter p_2 defines the geometry of this mechanism as shown in Fig. 3(a).

[7]The black region in Fig. 2(b) corresponds to the nonfeasible area in $\mathcal{K}_0 \times \mathcal{Q}_0$ space, whereas the white region corresponds to the output stiffnesses and the output positions that cannot be achieved.

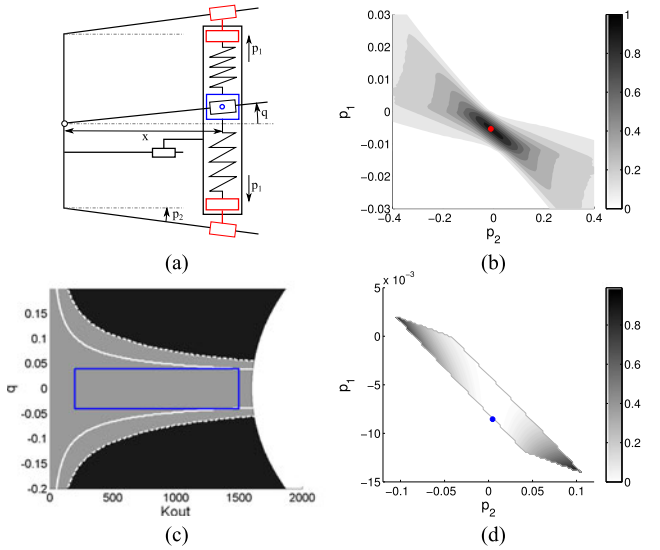

Fig. 3. (a) Schematic representation of the variable stiffness slider mechanism. In this mechanism, q denotes the output position whereas x denotes the motor position used to adjust the stiffness of the link. There are two linear springs embedded in the mechanism with stiffness constant k. The figure also shows the design parameters that define the tensioning of the springs p_1 and the geometry of the mechanism p_2. (b) Area of the feasible workspace as a function of the design parameters. The red dot indicates the largest area and the corresponding design parameters. (c) User-defined output workspace $\mathcal{K}_0 \times \mathcal{Q}_0$ (entire box), largest feasible workspace $\mathcal{S}_{\text{out}}(\mathbf{p}_{\max})$ (gray area) and desired workspace $\mathcal{S}_{\text{d, out}}$ (blue box). The white lines indicate the optimal feasible workspace. (d) Cost function (squared input force averaged over the desired workspace) as a function of the feasible parameters (gray scale). The optimal parameters are denoted with the blue dot.

The model of this mechanism is given by its potential energy function

$$V(x, q; \mathbf{p}) = \frac{1}{2} k \delta_+ (x, q; \mathbf{p})^2 + \frac{1}{2} k \delta_- (x, q; \mathbf{p})^2 \tag{15}$$

where $\delta_\pm = p_1 + x \tan(p_2) \pm x \tan(q)$ denotes the deformation of the springs. Similar to the previous example, we assume that the design is realized using compression springs, which have finite deformation limits [11]. The corresponding physical constraints (four inequality constraints)

$$\delta_+ (x, q; \mathbf{p}) \in [-0.012, 0] \text{ and } \delta_- (x, q; \mathbf{p}) \in [-0.012, 0] \tag{16}$$

ensure that the solution of the mathematical design formulation is realizable in practical application. Finally, the range of parameters and the workspace are defined by

$$\mathcal{P}_0 = [-0.03, 0.03] \times [-0.4, 0.4] \text{ and}$$
$$\mathcal{X}_0 \times \mathcal{Q}_0 \times \mathcal{K}_0 = [0, 0.1] \times [-0.2, 0.2] \times [0, 2000]. \tag{17}$$

The above design problem can be numerically solved following the procedure outlined in Section III. According to this procedure, the area of the feasible workspace is first maximized by solving (9). Fig. 3(b) shows the area of the workspace as a function of the design parameters (gray scale) and the maximal area (red dot) for $\mathbf{p} = \mathbf{p}_{\max}$. Fig. 3(c) (gray) shows the largest feasible workspace and the desired workspace chosen by the user: $\mathcal{S}_{\text{d, out}} = [200, 1500] \times [-0.04, 0.04]$ (blue box).

Using the desired workspace defined by the user, we solve the second optimization problem (12). The solution of this problem defines the design characterized by the lowest average input force over the desired workspace of the mechanism. This result is shown in Fig. 3(d) where the optimal parameters correspond to the blue dot. The total cost associated

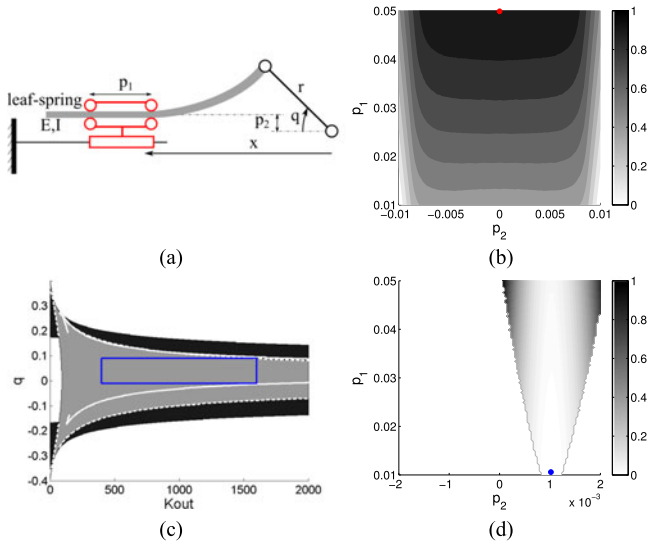

Fig. 4. (a) Schematic representation of the variable stiffness mechanism. The parameters used in the design optimization define the distance between the rollers p_1 and the offset of the rotation axis p_2. (b) Area of the feasible workspace. The largest feasible workspace is denoted with the red dot. (c) Largest feasible workspace (gray), desired workspace selected by the user (blue box) and optimal feasible workspace (white line). (d) Value of the cost function (squared input force averaged over the desired workspace) and the optimal parameters (blue dot).

with the optimal mechanism ($\mathbf{p} = \mathbf{p}^*$) is significantly lower than the cost associated with the nonoptimized mechanism (i.e., the one which has the largest feasible workspace $\mathbf{p} = \mathbf{p}_{\max}$)

$$\overline{F_{\text{in}}^2}(\mathbf{p}^*)/\overline{F_{\text{in}}^2}(\mathbf{p}_{\max}) \approx 0.12.$$

According to the above results, the optimal design is characterized by nonzero precompression of the springs $p_1^* < 0$ and zero inclination angle of the slider guides i.e., $p_2 = 0$. This second parameter allows the theoretical design to maintain a given stiffness setting with zero input force (provided the mechanism is at its undeflected configuration $q = 0$). It is this feature that has been recognized and exploited in [11] to realize an energy efficient variable stiffness actuator.

C. Variable Stiffness Leaf-Spring Mechanism

Figure 4(a) shows the third variable stiffness mechanism. In this mechanism, a leaf-spring is connected via a crank-shaft to the output link. As in some practical designs [3], [12], [24], the output stiffness of this mechanism can be changed by changing the effective length of the leaf-spring element. This is realized by moving the two rollers as shown in Fig. 4(a). We aim to find the optimal design for this mechanism with respect to two design parameters, one is the distance between the two rollers p_1, whereas the other is the eccentricity p_2 between the axis of the output link and the neutral axis of the undeflected leaf-spring, see Fig. 4(a).

Following the procedure established in the previous sections, we first define the parameterized model of this mechanism. This model is given by the following elastic potential energy function:[8]

$$V(x, q; \mathbf{p}) = \frac{3EI(r\sin(q) - p_2)^2}{2(x - r\cos(q))^2(p_1 + x - r\cos(q))} \tag{18}$$

[8]This model is valid in small deflection regime of the mechanism. For the chosen desired workspace, see Fig. 4(c) blue box, this model provides an adequate representation of the leaf-spring mechanism.

where E is Young's modulus of the leaf-spring material, I is the second moment of area of the spring while r is the radius of the crank-shaft shown in Fig. 4(a).

In the previous examples, the standard linear coil springs enabled us to express all physical constraints as deformation limits. A constraint of this type states that the stress inside the elastic element should not exceed the yield stress of the material used to make the elastic element. For the leaf-spring mechanism, this physical limitation is given by the following constraint:

$$\left|\frac{\sigma}{\sigma_y}\right| = \frac{3Eh}{2\sigma_y}\left|\frac{(r\sin(q) - p_2)}{(x - r\cos(q))(p_1 + x - r\cos(q))}\right| \leqslant 1 \tag{19}$$

where σ_y is the yield stress while h is the thickness of the leaf-spring.

The formulation is completed by providing the range of design parameters and the workspace

$$\mathcal{P}_0 = [0.01, 0.05] \times [-0.01, 0.01],$$
$$\mathcal{X}_0 \times \mathcal{Q}_0 \times \mathcal{K}_0 = [0.025, 0.05] \times [-0.4, 0.4] \times [0, 2000]. \tag{20}$$

As for the previous mechanisms, the first optimization algorithm (9) is used to find the largest feasible workspace. Fig. 4(b) shows the area of the feasible workspace as a function of the design parameters. The parameters that lead to the largest feasible workspace correspond to the red dot in Fig. 4(b). The largest feasible workspace (gray area) is shown in Fig. 4(c). The nonsymmetric desired workspace, chosen in this example, is represented by the blue box, i.e., $\mathcal{S}_{\text{d}} = [400, 1600] \times [-0.01, 0.09]$ in the same figure.

Using this desired workspace, the second optimization problem (12) was solved to find the design parameters. The distribution of the cost over the desired workspace is shown in Fig. 4(d). The parameters that correspond to the optimal mechanism are shown in the same plot with blue dot.

According to the result of the design optimization, the optimal mechanism should have nonzero eccentricity $p_2 \neq 0$. The cost associated with such nonsymmetric design ($\mathbf{p} = \mathbf{p}^*$) is remarkably low compared to the cost associated with the nonoptimized design

$$\overline{F_{\text{in}}^2}(\mathbf{p}^*)/\overline{F_{\text{in}}^2}(\mathbf{p}_{\max}) \approx 0.02.$$

Unlike in the first example (presented in Section IV-A), finding the optimal offset p_2 cannot be intuitively done in this example. The present approach can be used to numerical compute such parameter irrespective of the particular design.

V. Computational Comparison of Variable Stiffness Mechanisms

The previous section was dedicated to algorithmic design of variable stiffness mechanisms, i.e., optimal dimensional synthesis of variable stiffness mechanisms with predefined kinematic structure (topology). While this is an essential step toward automatic computational design, we aim to demonstrate the treatment of a more general problem, where we cross-compare dimensionally optimal designs which have different kinematic topology. We will illustrate here how to perform such comparison using the algorithmic formulation for design optimization presented in Section III.

The computational comparison of two topologically different designs will be shown using:

1) the cam mechanism described in Section IV-A and
2) the leaf-spring mechanism considered in Section IV-C.

In order to maximize the clarity of the presentation, the optimization is performed with two parameters. In particular, the first parameter $p_1^{\text{A,B}}$ is used for each of the mechanisms, whereas the second parameter is

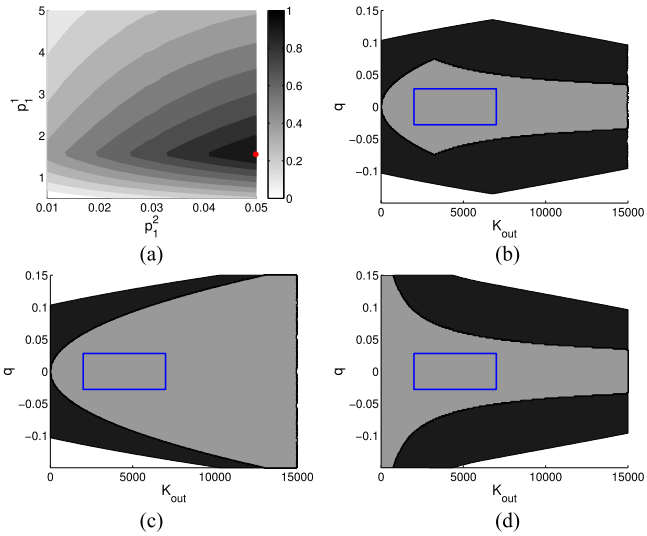

Fig. 5. (a) Area of the common feasible workspace. The largest common feasible workspace is denoted with the red dot. (b) Largest common feasible workspace (gray). (c) Largest feasible output workspace for the cam mechanism, i.e., $\mathcal{S}^{\mathrm{A}}_{\mathrm{out}}(\mathbf{p}^{\mathrm{A}}_{\mathrm{max}})$ (gray). (d) Largest feasible output workspace for the leaf-spring mechanism, i.e., $\mathcal{S}^{\mathrm{B}}_{\mathrm{out}}(\mathbf{p}^{\mathrm{B}}_{\mathrm{max}})$ (gray). In all three plots (b)–(d), the blue box represents the desired workspace $\mathcal{S}_{\mathrm{d,\,out}} = [2000, 7000] \times [-0.028, 0.028]$.

fixed to zero[9] $p_2^{\mathrm{A,B}} = 0$. In order to meaningfully compare these two topologically different mechanisms, a common output requirement has to be set for both of them. This is done here by comparing each mechanism's best performing design on a common desired workspace $\mathcal{S}_{\mathrm{d,\,out}}$. This problem is again broken down to two optimization problems. The first optimization problem is used to find the largest common feasible workspace:

$$\mathbf{p}_{\mathrm{max}} = \underset{(\mathbf{p}^{\mathrm{A}},\mathbf{p}^{\mathrm{B}})\in\mathcal{P}_0^{\mathrm{A}}\times\mathcal{P}_0^{\mathrm{B}}}{\operatorname{argmax}} \iint_{\mathcal{S}^{\mathrm{A}}_{\mathrm{out}}(\mathbf{p}^{\mathrm{A}})\cap\mathcal{S}^{\mathrm{B}}_{\mathrm{out}}(\mathbf{p}^{\mathrm{B}})} dK\,dq \tag{21}$$

where $(\mathbf{p}^{\mathrm{A}}, \mathbf{p}^{\mathrm{B}}) = (p_1^{\mathrm{A}}, p_1^{\mathrm{B}}) \in \mathcal{P}_0^{\mathrm{A}} \times \mathcal{P}_0^{\mathrm{B}}$ contains the parameters of both mechanisms while the feasible workspaces $\mathcal{S}^{\mathrm{A,B}}_{\mathrm{out}}(\mathbf{p}^{\mathrm{A,B}})$ are defined by (11). The above computation could be done using (6), but it is more convenient to use (21) because it is easier to define the intersection of the feasible workspaces $\mathcal{S}^{\mathrm{A}}_{\mathrm{out}} \cap \mathcal{S}^{\mathrm{B}}_{\mathrm{out}}$ in the output stiffness and output position space $(K, q) \in \mathcal{K}_0 \times \mathcal{Q}_0$ (since $\mathcal{S}^{\mathrm{A}}_{\mathrm{out}}$ and $\mathcal{S}^{\mathrm{B}}_{\mathrm{out}}$ are defined in that space by the user).

Figure 5(a) (red dot) shows the largest area of the common workspace. The largest common feasible workspace between these two mechanisms $\mathcal{S}^{\mathrm{A}}_{\mathrm{out}}(\mathbf{p}^{\mathrm{A}}_{\mathrm{max}}) \cap \mathcal{S}^{\mathrm{B}}_{\mathrm{out}}(\mathbf{p}^{\mathrm{B}}_{\mathrm{max}})$ is shown in Fig. 5(b) (gray area). This area is obtained by the intersection of the feasible workspaces of the two mechanisms shown in Fig. 5(c)–(d). In all these figures, the blue boxes show the user-defined desired output workspace $\mathcal{S}_{\mathrm{d,\,out}}$.

Using this workspace, we solved the second optimization problem (12), as in Sections IV-A and IV-C. The result of this optimization is shown in Fig. 6. The optimal design parameters are denoted with blue dots in these figures.

According to the numerical computation, the optimal cost is approximately five times larger for the optimized cam mechanism compared to the optimized leaf-spring mechanism:

$$\overline{F^2_{\mathrm{in}}}^{\mathrm{B}}(\mathbf{p}^{\mathrm{B}*}) / \overline{F^2_{\mathrm{in}}}^{\mathrm{A}}(\mathbf{p}^{\mathrm{A}*}) \approx 0.2.$$

This indicates an energetic advantage of the leaf-spring mechanism. We note that the result of this quantitative comparison depends on:

[9]This is the optimal solution if the desired workspace is symmetric.

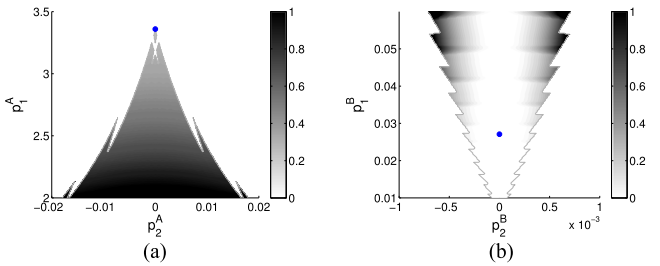

Fig. 6. Optimization of the (a) cam mechanism and the (b) leaf-spring mechanism for the same desired workspace $\mathcal{S}_{\mathrm{d,\,out}}$. The color code is the same in these two plots. The cost at the optimal solution is ~ 5 times lower for the leaf-spring mechanism compared to the cam mechanism.

(i) the user-selected parameter space, (ii) the desired workspace, and (iii) the physical parameters that are not optimized. Regardless of this, the proposed formulation provides an objective way to computationally cross-compare mechanisms that have topologically different kinematic structure.

The proposed computational design approach presents the first step toward automatic design of variable stiffness mechanisms. In the same way as it was shown here for two mechanisms, the comparison between a large number of mechanisms can be performed in a predefined library. Such comparison is the key to realize automatic computational design for variable stiffness, and possibly other, mechanisms.

VI. Application to Mechanism Design

In this section, we use the proposed framework to optimize the design of the variable stiffness leaf-spring mechanism presented in [12]. In order to do this, we simultaneously optimize four design parameters: the distance between the two rollers of the slider p_1, the length of the crank-shaft p_2, the width of the leaf-springs p_3, and the thickness of a single leaf p_4 in the stack of leaf-springs, as shown in Fig. 7(a). By optimizing these parameters, we aim to achieve large range, and low power drain stiffness modulation when using this mechanism to emulate a human ankle joint.

A. Design Optimization

The behavior of the human ankle joint was characterized using experimental data (angle and torque) reported in [25]. Using these data, we defined the largest output workspace $\mathcal{K}_0 \times \mathcal{Q}_0 = [0, 2000]$ N·m/rad $\times[-0.4, +0.4]$ rad. The value of the average ankle stiffness was then estimated during the gait cycle by the slope of the plot representing the ankle torque versus the ankle angle. This estimation lead to the following results: (i) when the foot is in the air—swing phase—the stiffness of the ankle is low $K_{\mathrm{out}} \approx 10$ N·m/rad, while the range of motion is relatively large $q \in [-0.35, +0.35]$ rad, while (ii) when the foot is on the ground—stance phase—the stiffness assumes higher values, up to $K_{\mathrm{out}} \approx 1200$ N·m/rad and the motion is reduced $q \in [-0.15, +0.15]$ rad. We use this information to set up the desired workspace within the largest feasible workspace of the mechanism $\mathcal{S}_{\mathrm{d,\,out}} \subseteq \mathcal{S}_{\mathrm{out}}(\mathbf{p}_{\mathrm{max}})$. This desired workspace $\mathcal{S}_{\mathrm{d,\,out}}$, represented by a union of two trapezoidal shapes, is depicted with blue lines in Fig. 7(b).

In order to find the optimal design parameters $\mathbf{p}^* \in \mathcal{P}_0 = [10, 50] \times [5, 50] \times [5, 20] \times [0.5, 1.5]$ mm—thous that lead to the most power saving design—we solve (12). The solution of this problem is given by: $\mathbf{p}^* = [48.5, 13.0, 19.9, 1.5]$ mm. The feasible workspace and the desired workspace for the optimal mechanism ($\mathbf{p}^*$ solid lines) and the mechanism with the largest feasible workspace ($\mathbf{p}_{\mathrm{max}}$ dashed lines) is shown in Fig. 7(b) and Fig. 7(c).

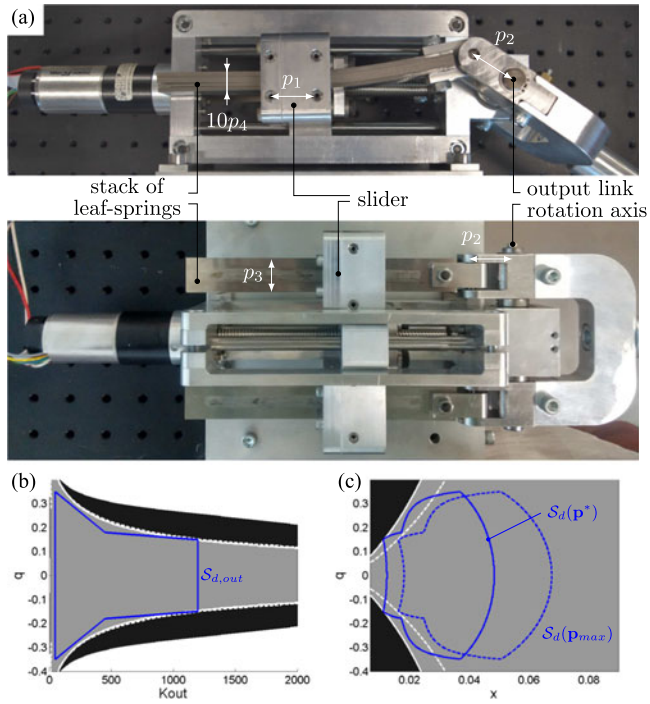

Fig. 7. (a) Prototype variable stiffness leaf-spring mechanism. (b) Feasible output workspace (K_{out}, q) for the optimal parameters $\mathbf{p}^*$ (gray). The boundary of this workspace is shown with white lines. The white dashed lines denote the boundary of the largest feasible workspace. The blue lines show the user-defined desired workspace. (c) Workspaces of the optimal mechanism (solid lines) and the one with the largest feasible workspace (dashed lines) in (x, q) space.

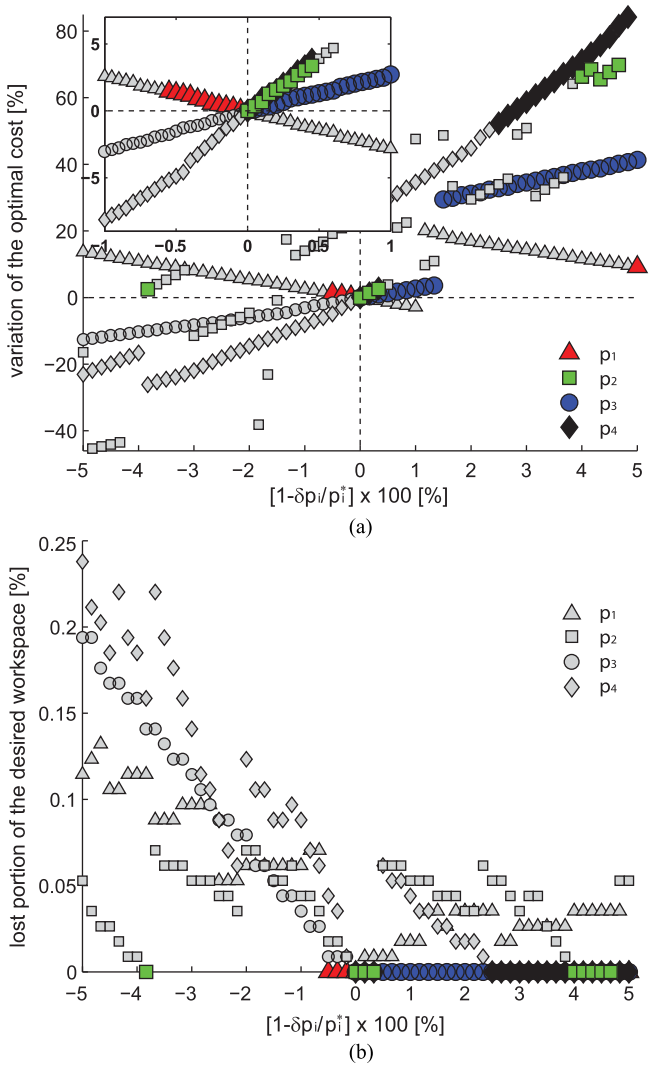

Fig. 8. Variable length leaf-spring design. (a) Effect of parameter variation on the cost: $(1 - \overline{F_{\text{in}}^2}(\mathbf{p}^* + \delta\mathbf{p})/\overline{F_{\text{in}}^2}(\mathbf{p}^*)) \times 100\%$. Colored markers represent parameter variations that preserve the desired workspace while the gray markers represent parameter variations for which the feasible workspace does not fully contain the desired workspace. (b) Area of the lost desired workspace due to variation of the design parameters: $(1 - \text{area}[\mathcal{S}_{\text{out}}(\mathbf{p}^* + \delta\mathbf{p}) \cap \mathcal{S}_{\text{d, out}}]/\text{area}[\mathcal{S}_{\text{d, out}}]) \times 100\%$. The lost area corresponds to high stiffnesses and large output angles in the desired workspace [i.e., right corners of the blue polygon in Fig. 7(b)]. (a) The inset shows that the cost cannot be reduced by feasible parameter variations.

According to Fig. 7(b) and Fig. 7(c), there are three apparent differences between the optimal mechanism and the mechanism that has the largest feasible workspace. These are summarized in the following: (i) compared to the design that has the maximal feasible workspace, only a small region of the workspace (x, q) is nonfeasible for the optimal design (defined by white lines), see Fig. 7(c); (ii) the optimal design requires 27% smaller motion range for the slider, see Fig. 7(c), which translates to a considerably smaller mechanism. And finally, according to our calculations, (iii) the optimal mechanism will reduce the cost—average squared input force over the desired workspace—by 90% compared to the current prototype (which is the design that has the largest feasible workspace)

$$\overline{F_{\text{in}}^2}(\mathbf{p}^*)/\overline{F_{\text{in}}^2}(\mathbf{p}_{\text{max}}) \approx 0.1.$$

These result were obtained using the proposed formulation via systematic numerical optimization.

B. Robustness and Sensitivity of the Optimal Design

Quantifying how *imperfections in fabrication* affect the optimal design solution becomes important when it comes to practical realization. In this section, we investigate the effect of imperfections in the design parameters $\delta\mathbf{p}$ (e.g., due to inexact fabrication) on the proposed optimal leaf-spring design. In order to do this, we aim to quantify the influence of parameter variation on the (a) cost function $\overline{F_{\text{in}}^2}(\mathbf{p}^* + \delta\mathbf{p})$ and the (b) workspace $\mathcal{S}_{\text{out}}(\mathbf{p}^* + \delta\mathbf{p})$ of the optimal design. The result of this investigation is summarized in Fig. 8.

Figure 8(a) shows the variation of the cost with respect to the design parameters near to the optimal solution. The four different markers are associated with the four optimized parameters. The colored markers denote the parameters for which the feasible workspace contains the desired workspace, i.e., $\mathcal{S}_{\text{d, out}} \subseteq \mathcal{S}_{\text{out}}(\mathbf{p})$, whereas the gray markers represent the parameters for which the feasible workspace does not fully contain the desired workspace, i.e., $\mathcal{S}_{\text{d, out}} \nsubseteq \mathcal{S}_{\text{out}}(\mathbf{p})$. One can see that small variation of the parameters $(\pm 5\%)$ leads to large increase in the objective function $(> 80\%)$. This highlights the importance of the design optimization proposed in this paper. It can be also observed that the workspace of the mechanism only remains feasible under $[0, 5\%]$ variation of p_3, and less than 1% variation of the other three parameters, i.e., p_1, p_2, and p_4. This means that the desired workspace may not be achieved even under relatively small variations of the optimal design parameters.

Figure 8(b) shows the percentage of the lost desired workspace as a function of the design parameters. We observe that $\pm 5\%$ variation of the design parameters leads to small $(< 0.25\%)$ difference between

the feasible and the desired workspace. These results collectively indicate that $\pm 0.5\%$ variation of the parameters leads to negligible loss in the workspace ($< 0.125\%$) and less than 10% increase in the cost [for most of the parameter variations, see the inset in Fig. 8(a)]. The $\pm 0.5\%$ variation in the parameters is achievable using standard fabrication approaches. This enables near-optimal practical realization of the computed optimal leaf-spring design.

Beside understanding the effect of design imperfections, the above analysis may also be used to identify the sensitivity of each individual parameter on the optimal design. In turn, we can observe that p_1 and p_3 have similar sensitivity while the influence of p_2 and p_4 on the cost is nearly three times higher, see Fig. 8(a). This information can be useful, namely, it can guide the designer in how to select the most important parameters for a given design. When considering the leaf-spring design, this analysis suggests that one may reduce the computational complexity of the optimization by limiting the numerical search to the two most sensitive parameters. These parameters denote the length of the crank shaft p_2 and the thickness of a single leaf p_4 in the leaf-spring design, see Fig. 7(a).

The examples considered in this paper consistently show that optimization of limited number of parameters can generate high improvements in the mechanism's power requirement compared to the case when no such optimization is performed. While choosing the design parameters in the proposed formulation is nontrivial, the analysis presented in this section provides a computational tool to find the parameters that have the most influence on the design.

VII. Conclusion

In this paper, we presented a novel optimization-based algorithmic framework for the design of variable stiffness mechanisms. We focused on dimensional synthesis of different types of mechanisms to achieve low-power stiffness modulation through optimal mechanical design. A semiautomatic design pipeline is described with a detailed mathematical formulation for the dimensional synthesis of variable stiffness designs. This formulation was used to compute optimal design parameters for three qualitatively different mechanisms inspired by existing mechanical designs. We have also demonstrated how to perform simultaneous dimensional and topological synthesis to find a variable stiffness mechanism that requires the least power by design. We foresee the proposed formulation to enable algorithmic design from first principles, capable of addressing nonintuitive design problems; thous that had been long identified challenging to treat using experience based or more classical computational approaches.

References

[1] R. van Ham, T. G. Sugar, B. Vanderborght, K. W. Hollander, and D. Lefeber, "Compliant actuator designs," *IEEE Robot. Autom. Mag.*, vol. 16, no. 3, pp. 81–94, Sep. 2009.

[2] K. F. Laurin-Kovitz, J. E. Colgate, and S. D. R. Carnes, "Design of components for programmable passive impedance," in *Proc. IEEE Int. Conf. Robot. Autom.*, vol. 2, Sacramento, CA, USA, Apr. 1991, pp. 1476–1481.

[3] T. Morita and S. Sugano, "Design and development of a new robot joint using a mechanical impedance adjuster," in *Proc. IEEE Int. Conf. Robot. Autom.*, vol. 3, Nagoya, Japan, May 1995, pp. 2469–2475.

[4] C. E. English, "Implementation of variable joint stiffness through antagonistic actuation using rolamite springs," *Mech. Mach. Theory*, vol. 341, no. 1, pp. 27–40, 1999.

[5] S. Wolf and G. Hirzinger, "A new variable stiffness design: Matching requirements of the next robot generation," in *Proc. IEEE Int. Conf. Robot. Autom.*, Pasadena, CA, USA, May 2008, pp. 1741–1746.

[6] J. W. Hurst, J. Chestnutt, and A. A. Rizzi, "The actuator with mechanically adjustable series compliance," *IEEE Trans. Robot.*, vol. 26, no. 4, pp. 597–606, Aug. 2010.

[7] F. Petit, M. Chalon, W. Friedl, M. Grebenstein, A. Albu-Schaffer, and G. Hirzinger, "Bidirectional antagonistic variable stiffness actuation: Analysis, design and implementation," in *Proc. IEEE Int. Conf. Robot. Autom.*, Anchorage, AK, USA, May 2010, pp. 4189–4196.

[8] L. C. Visser, R. Carloni, and S. Stramigioli, "Energy-efficient variable stiffness actuators," *IEEE Trans. Robot.*, vol. 27, no. 5, pp. 865–875, Oct. 2011.

[9] R. Carloni, L. C. Visser, and S. Stramigioli, "Variable stiffness actuators: A port-based power-flow analysis," *IEEE Trans. Robot.*, vol. 28, no. 1, pp. 1–11, Feb. 2012.

[10] T.-H. Chong, V. Chalvet, and D. J. Braun, "Analytical conditions for the design of variable stiffness mechanisms," in *Proc. IEEE Int. Conf. Robot. Autom.*, Singapore, May 2017, pp. 1241–1247.

[11] A. Jafari, N. G. Tsagarakis, and D. G. Caldwell, "A novel intrinsically energy efficient actuator with adjustable stiffness (AwAS)," *IEEE/ASME Trans. Mechatronics*, vol. 18, no. 1, pp. 355–365, Feb. 2013.

[12] D. J. Braun, S. Apte, O. Adiyatov, A. Dahiya, and N. Hogan, "Compliant actuation for energy efficient impedance modulation," in *Proc. IEEE Int. Conf. Robot. Autom.*, Stockholm, Sweden, May 2016, pp. 636–641.

[13] A. Dahiya and D. J. Braun, "Efficiently tuneable positive-negative stiffness actuator," in *Proc. IEEE Int. Conf. Robot. Autom.*, Singapore, May 2017, pp. 1235–1240.

[14] E. Ferguson, "The mind's eye: Nonverbal thought in technology," *Science*, vol. 197, pp. 827–836, 1977.

[15] F. Freudenstein and G. N. Sandor, "Synthesis of path generating mechanisms by means of a programmed digital computer," *ASME J. Eng. Ind.*, vol. 81, no. 1, pp. 159–168, 1959.

[16] R. S. Hartenberg and J. Denavit, *Kinematic Synthesis of Linkages*. New York, NY, USA: McGraw-Hill, 1964.

[17] J. M. McCarthy and G. S. Soh, *Geometric Design of Linkages*, 2nd ed. New York, NY, USA: Springer-Verlag, 2010.

[18] H. A. Eschenauer and N. Olhoff, "Topology optimization of continuum structures: A review," *Appl. Mech. Rev.*, vol. 54, no. 4, pp. 331–390, 2001.

[19] L. L. Howell, *Compliant Mechanisms*. Hoboken, NJ, USA: Wiley, 2001.

[20] D. J. Braun *et al.*, "Robots driven by compliant actuators: Optimal control under actuation constraints," *IEEE Trans. Robot.*, vol. 29, no. 5, pp. 1085–1101, Oct. 2013.

[21] R. van Ham, B. Vanderborght, M. van Damme, B. Verrelst, and D. Lefeber, "MACCEPA, the mechanically adjustable compliance and controllable equilibrium position actuator: Design and implementation in a biped robot," *Robot. Auton. Syst.*, vol. 55, no. 10, pp. 761–768, 2007.

[22] V. Chalvet and D. J. Braun, "Criterion for the design of low power variable stiffness mechanisms," *IEEE Trans. Robot.*, vol. 32, no. 4, pp. 1002–1010, Aug. 2017.

[23] B.-S. Kim and J.-B. Song, "Design and control of a variable stiffness actuator based on adjustable moment arm," *IEEE Trans. Robot.*, vol. 28, no. 5, pp. 1145–1151, Oct. 2012.

[24] J. Choi, S. Hong, W. Lee, S. Kang, and M. Kim, "A robot joint with variable stiffness using leaf springs," *IEEE Trans. Robot.*, vol. 27, no. 2, pp. 229–238, Apr. 2011.

[25] M. Kadaba, H. Ramakrishnan, M. Wootten, J. Gainey, G. Gorton, and G. Cochran, "Repeatability of kinematic, kinetic, and electromyographic data in normal adult gait," *J. Orthopaedic Res.*, vol. 7, no. 6, pp. 849–860, 1989.